International Journal of Mechanical and Production Engineering Research and Development (IJMPERD)
ISSN (P): 2249–6890; ISSN (E): 2249–8001
Vol. 9, Issue 4, Aug 2019, 1335–1342

EFFECT OF POST-WELD HEAT TREATMENT ON DISSIMILAR FRICTION STIR WELDED AA6082 AND A319 ALUMINIUM ALLOYS

V. ANAND KUMAR[1] & N. GOVIND[2]

[1]*Research Scholar, Department of Mechanical Engineering, ANU College of Engineering, Andhra Pradesh, India*

[2]*Associate Professor, Department of Mechanical Engineering, RVR & JC College of Engineering, Andhra Pradesh, India*

ABSTRACT

The effects of post-weld heat management at a solution temperature of 540°C for 5 hrs 30 mins continuing by ageing at 190°C for 6 hrs on microstructure and mechanical properties of friction stir welded different aluminium alloys A319 and AA6082 have been examined. Post-weld ageing results in enhanced mechanical properties. The outcome of ageing on the morphology of the subsequent phase particles of silicon, copper along with iron in the fold zone has been studied. The hardness of the fold zone for both as-welded and post-weld ageing was found to be lower than that of AA6082 but higher than A319 base metal. Microstructural studies reveal that the A319 dominates the fold zone.

KEYWORDS: Friction Stir Welding, Aluminium Alloys, Post Weld Heat Treatment, Intermetallics & Mechanical Properties

Received: Jun 01, 2019; **Accepted**: Jun 20, 2019; **Published**: Aug 02, 2019; **Paper Id.**: IJMPERDAUG2019138

Original Article

1. INTRODUCTION

Friction stir welding (FSW) is a hard state welding method invented and patented by the Welding Institute (TWI) in 1991, Ref. [1]. FSW overcomes many welding problems of fusion welded aluminium alloys such as porosity, precipitates resolution, solidification cracking etc. The superiority of the FSW joint depends on the development parameters including rotation speed, welding speed and axial load. The general issues of dissimilar alloy FSW are the formation of the secondary precipitates, variations in mechanical properties and different deformation behaviour, Ref. [2]. A319 alloys are used in automotive cylinder heads, engine manifolds and aircraft components. AA6082 has wide applications in the transport and construction industries. Both AA6082 and A319 have high corrosion resistance, heat treatability, Weldability and cold forming properties, Ref. [3]. Although many studies of dissimilar aluminium alloys have been focused on the mechanical and microstructural aspects, the result of post-weld ageing on dissimilar FSW of A319 and AA6082 has not yet been identified. The current study investigates the effects of as-welded (AW) and post-weld heat treatment (PWHT) environment on microstructure and mechanical properties of the dissimilar friction stir welded AA6082 and A319 aluminium alloys.

2. EXPERIMENTAL WORK

The materials owned in this study were wrought aluminium alloy 6082-T6, procured as rolled product and cast aluminium alloy A319.0, available as an ingot. The plates were sliced to the required proportions of 100 mm ×50 mm× 6 mm plates. The chemical components and mechanical properties of the standard metals are given in Table 1 and Table 2. FSW was conducted on an FSW machine supplied by R. V. Machine Tools,

Coimbatore, India. The FSW tool comprises a direct square pin profile tool made of M2- HSS, hardened to 60 Hv. The tool carry diameter was 18 mm and the pin length was 5.7 mm. The welding parameters were chosen as 800, 1000 and 1300 rpm as revolving speed keeping welding speed and axial load as constant at 60 mm. min–1 and 6 kN correspondingly. A319 was kept on the approaching side and AA6082 was kept on the receding side. The welded plates were cut into two equal halves transverse to the weld direction and one half was used for PWHT. The weldments are heat-treated at the temperature of 540°C for 5 hrs 30 min continuing by quenching in the water at atmospheric temperature and artificial ageing at 190°C for 6 hrs.

Table 1: Mechanical Properties of AA6082 and A319 Aluminium Alloys

BM	UTS (MPa)	YS (MPa)	E (%)	Hardness (Hv)
A319	186	124	12	85
AA6082	248	219	2.8	90
UTS-Ultimate Tensile Strength, YS-Yield Strength, E (%) – Percentage of elongation				

Table 2: Comparision of Parent Metals AA6082 and A319

Base metals	Si	Cu	Mg	Mn	Ti	Zn	Fe	OT	Al
AA6082	1.1	0.1	0.9	0.6	0.1	0.2	0.5	0.25	Bal.
A319	6	3.4	0.1	0.5	0.25	0.1	1	0.35	Bal.

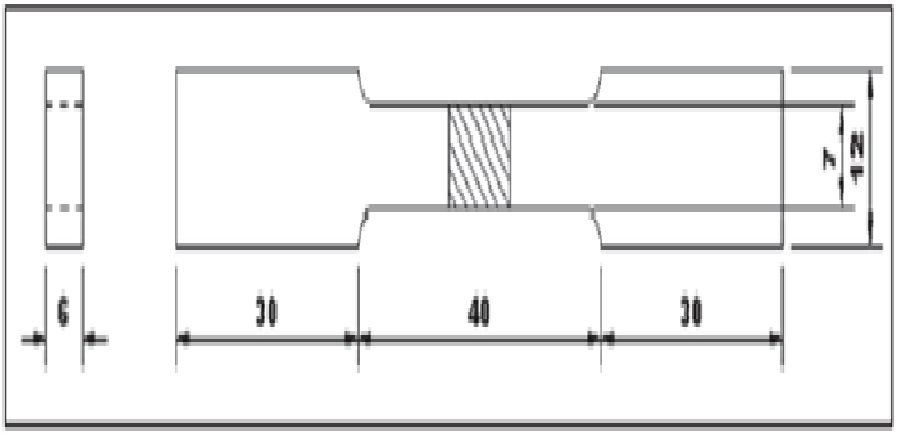

Figure 1: Tensile Specimen as per ASTM E8-M04

Tensile tests are conducted as per (ASTM E8-M04) standards as shown in Figure 1 on an electromechanically controlled universal testing machine (Make: FIE Bluestar, India; Model: UNITEK-94100). Vickers microhardness tests were conducted using a Vickers microhardness tester (MMT-X7 Matzusawa, Japan) by impacting a weight of 0.5 kg for 10 s at various locations of the FSW zones. Samples were mechanically positioned with various grits and refined with diamond paste. The chemical etching was performed using Keller's reagent. A scanning electron microscope (SEM) analysis was done by using a MEJI, Japan, Model: MIL- 7100 to characterize the various zones of the weldments.

The grain size measurement of the support metal and the nugget zone was calculated as per ASTM E-112 standard using image analyzing software with a magnification of 400 ×. The maximum number of fields for analysis was around 4 to 7 and the mean of the grain size was taken into account.

3. RESULTS AND DISCUSSIONS

3.1. Microstructural Properties

The device and the workpiece interaction concern the fragmentation and distribution of second phase precipitates within the stir zone (SZ), Ref. [4]. FSW produces seven macro structurally distinct regions across the weld as 1) base metal (BM)-AA6082, 2) heat-affected zone (HAZ)-AA6082, 3) thermo-mechanically affected zone (TMAZ)-AA6082, 4) stir zone, 5) TMAZ-A319, 6) HAZ-A319 and 7) BMA319. Figure 2a shows the microstructure of the cross-sectional area of the welded joint formed at 1300 rpm. A3xx alloys are characterized as Al – Si – Cu alloys, with Si and Cu forming the secondary phases. Cu in Al – Si – Cu alloys is present in the phases of Al_2Cu or Al – Al_2Cu – Si. Figure 2b shows the small blocky shape of the Al_2Cu precipitate in the BM A319. Based on literature studies, Refs. [5, 6], it has been identified that in the existence of iron, copper forms a blocky contour or finely distributed Al and $CuAl_2$ particles within the interdendritic regions. These blocky $CuAl_2$ phase particles do not dissolve during solid precipitation hardening but form eutectic-like deposits, as shown in Figure 2c. The distribution of silicon particles was homogeneous throughout the SZ at 1300 rpm compared to 800 and1000 rpm. Silicon is characterized in the BM as dark grey with a very irregular shape, as seen in Figure 3 b-AlFeSi, In Figure 4a it is identified as sharp needles shape. It forms a very weak bond with the matrix; it usually occurs near the a + Al_2Cu + AlCuMgSi + b eutectics, Ref. [7]. Previous studies Ref. [8] have shown that the mechanical properties of the alloy decrease with the rise in the Fe concentration above 0.5 %. The presence of a precipitate free zone (PFZ) as shown in Figure 4a is due to the dissolution of secondary phases at high temperature that arises during welding. The intermetallic phases of iron as skeleton shape were not identified at the weld joints after PWHT. Instead, the presence of intermetallics in the shape of Chinese script precipitates was found, as shown in Figure 4b. From the SEM image in Figure 5, it can be identified that after solution hardening, Al – Al_2Cu – Si phase dissolved to separate Al_2Cu particles as round globules. Also, the reprecipitation of silicon dendrites can be seen from the SEM microstructure in Figure 5. The grain size of AW varies from 5 ± 2 lm in the SZ whereas the PWHT specimens have the grain size distribution of 6 ± 2 lm in the SZ. AA6082 BM has an average grain size of 75 ± 53 lm whereas A319 has 176 ± 66 lm. The distribution of silicon is uniform throughout the SZ. The modification of silicon in the eutectic affects the mechanical properties of the joints. According to the phase diagrams of Al – Si – Cu – Fe, aluminium and silica will beat equilibrium with three phases Al_5FeSi, Al_2Cu and $Al15Mn_3Si_2$, Refs. [4–9]. 6xxx alloys are categorized by the secondary precipitates of Mg_2Si and Al_5FeSi phases in the base metal region along with the a-Al primary phase.

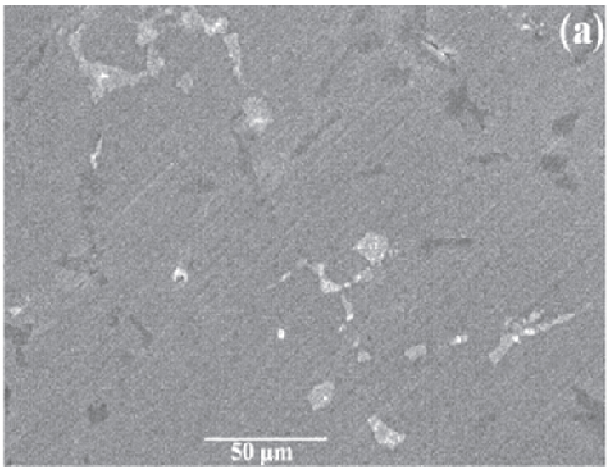

Figure 2(a): SEM Images of AA6082 at SZ

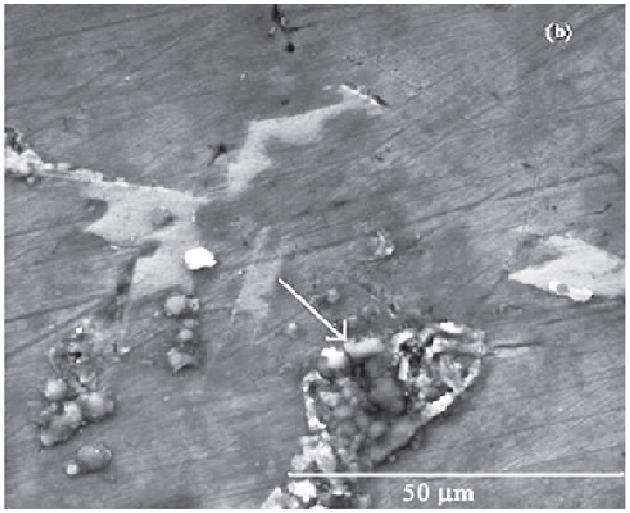

Figure 2(b): SEM Images of Base Metal A319 Containing Blocky Al_2Cu Phase

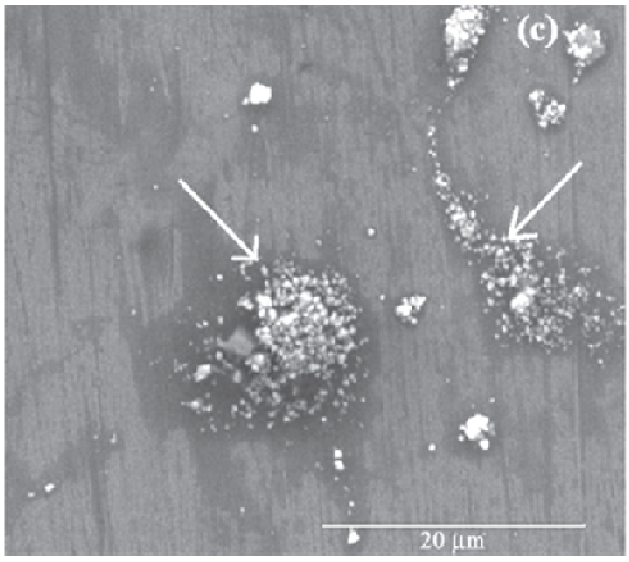

Figure 2(c): Presence of Blocky $CuAl_2$ Phase Particles after PWHT

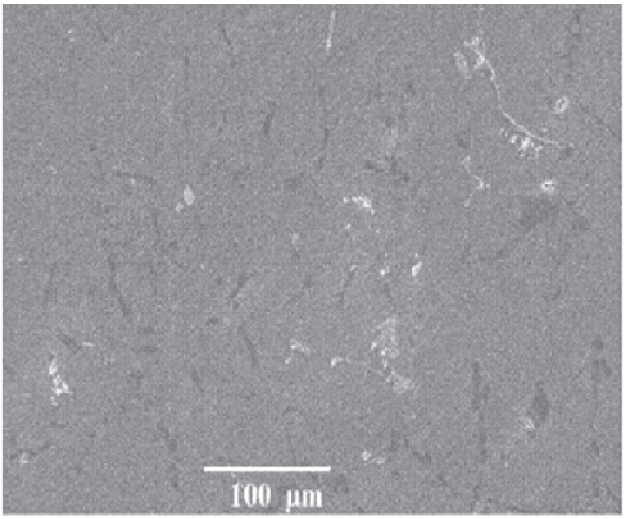

Figure 3: Distribution of Silicon Particles at SZ at 1300 rpm

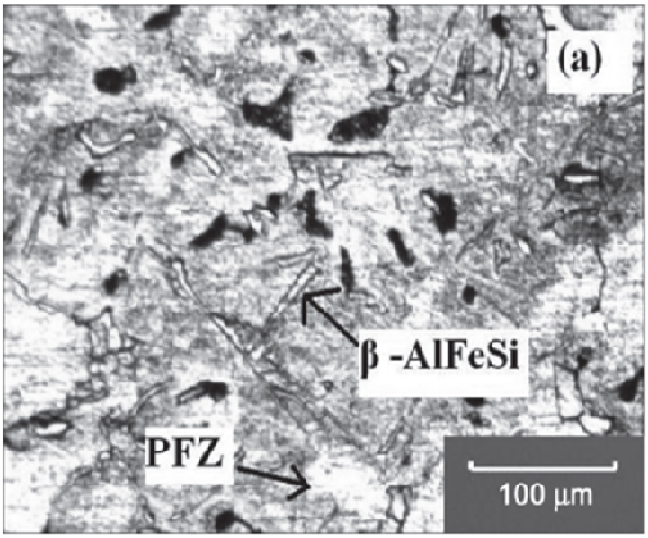

Figure 4 (a): Presence of Precipitates in the SZ at 1300 rpm in the AW Condition

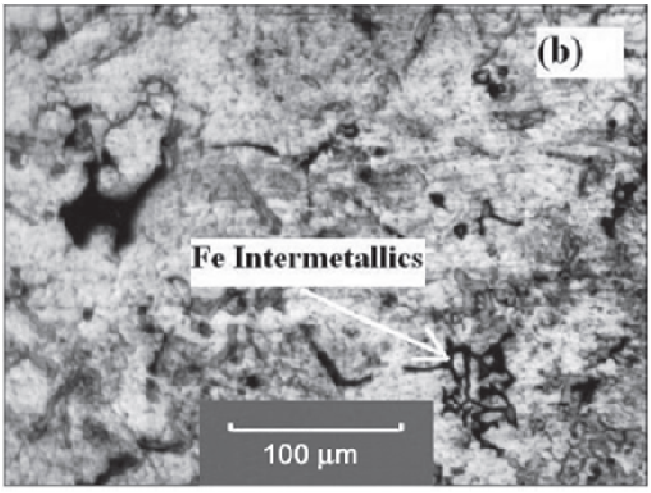

Figure 4 (b): PWHT towards A319 side in the SZ at 1300 rpm in the AW Condition

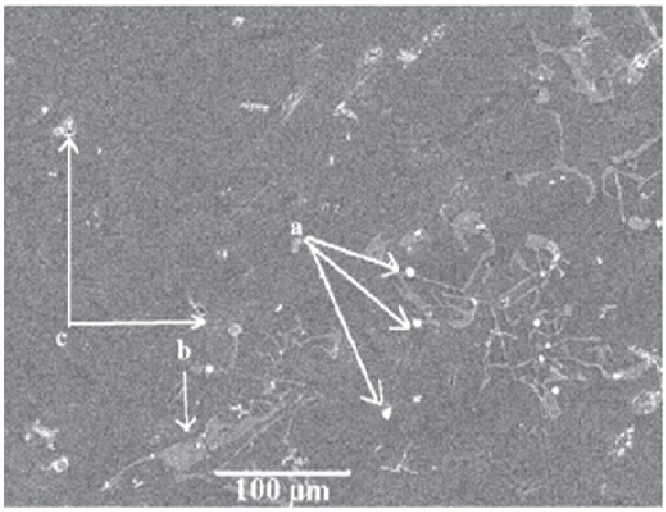

Figure 5: SZ at 1300 rpm after PWHT (a) Dissolution of Al_2Cu Precipitates, (b) Reprecipitation of Dendritic Al_2Si Alloys (c) Voids

3.2. Tensile Properties

The tensile specimens of the dissimilar FSW welds always broke at the A319 side except for the specimen produced at 800 rpm. This can be attributed to the lower yield strength of the A319 BM and due to the inherent defects that may arise during the casting process. Lee et al. [10] have confirmed that the dominant microstructure in the SZ plays an important role in lowering the strength of the SZ. The tensile values of the dissimilar weldments are shown in Table 3. The FSW yields a better quality weld without any defects at 1 300 rpm. PWHT gives better tensile values than AW weldments.

Table 3: Comparison of Mechanical Properties of AW and PWHT of the Dissimilar FSW Joints

RPM	AW			PWHT		
	YS(MPa)	UTS(MPa)	E(%)	YS(MPa)	UTS(MPa)	E(%)
800	71	90	8.5	101	116	13.7
1000	87	101	7.6	106	119	9.1
1300`	1	111	16.1	123	154	18.9

The results show more characteristics of A319 alloy than AA6082 alloy. The presence of burrow defect at the top of the A319 side at 800 rpm is due to insufficient plasticization of the materials at the given rotating speed. Also, a pinhole at the bottom of the A319 side at 1000 rpm may be attributed at abnormal stirring which lowers the tensile strength. Reference [11] suggests that the tensile strengths of dissimilar joints are affected due to the difference in material flow characteristics of the wrought and cast aluminium alloys.

3.3. Hardness Properties

The hardness values at the SZ are found to be lower than that of the AA6082 side but higher than A319 for both AW and PWHT conditions. PWHT results in an increase in hardness greater than 30–60 Hv in the overall weld. The grain size and impulsive allocation are the important factors in the microhardness distribution of precipitation hardening aluminium alloy. Ghosh et al. [12] suggest that though the welding process softens the region around the weld line which reduces hardness, fine recrystallized grain structure at the SZ aids in nugget hardness recovery. The breaking of secondary phase b precipitates due to higher dynamic recrystallization of the well grain structure during FSW is the key reason for the hardening of the SZ.

4. CONCLUSIONS

AA 6082 and A319 were successfully FS welded with different tool rotation speeds. Maximum tensile strength was achieved at 1300 rpm for the PWHT weldment. It has been found that the SZ is dominated by the advancing side alloy A319. The complete disbanding of Mg_2Si and the reprecipitation $CuAl_2$ as round globules and the presence of Chinese script shapes of b-Fe precipitates were identified with the PWHT. Homogenization of second phase particles in the SZ results in an enhancement in ductility and thus increases in the tensile strength. The hardness profiles of PWHT samples show higher hardness during the weld compared to the AW specimen. The hardness distribution at the NZ was lower than that of the BM AA6082 but higher than A319 BM.

REFERENCES

1. *R. S. Mishra, Z. Y. Ma: Mater. Sci. Eng. R50 (2005) 1–78. DOI:10.1016/j.mser. 2005.07.001*
2. *Y. C. Chen, K. Nakata: Scr. Mater. 58 (2008) 433–436. DOI:10.1016/j.scriptamat. 2007.10.033*
3. *S. Sayer, V. Ceyhun, O. Tezcan: Kovove Mater – Metall. Mater 46 (2008) 157–164.*
4. *K. Labisz, M. Krupinski, L. A. Dobrzanski: JAMME 37 (2009) 309–316.*
5. *F. H. Samuel, A. M. Samuel, H. W. Doty: AFS Trans. 104 (1996) 893.*
6. *Z. Hu, S. Yuan, X. Wang, G. Liu, Y. X. Huang: Mater. Des. 32 (2011) 5055–5060. DOI:10.1016/j.matdes.2010.12.007*
7. *L. Bäckerud, E. Król, J. Tamminen: Solidification Characteristics of Aluminum Alloys, Universitetsforlaget Oslo 1 (1986) p. 119.*
8. *Yunus, M. O. H. A. M. M. E. D., & Alsoufi, M. S. (2015). A statistical analysis of joint strength of dissimilar aluminium alloys formed by friction stir welding using taguchi design approach, anova for the optimization of process parameters. IMPACT: International Journal of Research in Engineering & Technology (IMPACT: IJRET), 3(7), 63–70.*
9. *L. Hurtalová, E. Tillová, M. Chalupová: Acta Metall. Slovaca- Conference 3 (2013)196–201. DOI:10.12776/amsc.v3i0.108*
10. *M. H. Mulazimoglu, N. Tenekedjiev, B. M. Closset, J. E. Gruzleski: Cast Metals 6 (1993) 16–28.*
11. *W. B. Lee, Y. M. Yeon, S. B. Jung: J. Mater. Sci. 38 (2003) 4183–4191. DOI:10.1023/A:1021892411067*
12. *M. Jayaraman, R. Sivasubramanian, V. Balasubramanian: J. Mater. Sci. Technol. 25 (2009) 655.*
13. *Cicek, V. O. L. K. A. N., & Ozdemir, M. E. H. M. E. T. (1). Characterization Studies of Aqueous Immersion Solutions of Novel Environmentally Friendly Organometallic Corrosion Inhibitors used to Cure Aluminum 2024, 6061, AND 7075 Alloys Substrates in Corrosive Media. International J. of General Engineering and Technology (IJGET), 2 (2), 1, 16.*
14. *M. Ghosh, K. Kumar, S. V. Kailas, A. K. Ray: Mater. Des. 31 (2010) 3033–3037, DOI:10.1016/j.matdes.2010.01.028*